ELSEVIER

Physica D 99 (1996) 252–268

PHYSICA D

A bound on the decay of defect–defect correlation functions in two-dimensional complex order parameter equations

Bruce W. Roberts *, Eberhard Bodenschatz, James P. Sethna

Laboratory of Atomic and Solid-State Physics, Cornell University, Ithaca, NY 14853-2501, USA

Received 10 April 1995; revised 22 February 1996; accepted 30 April 1996
Communicated by P. Kolodner

Abstract

Motivated by generic scale invariance, we examine the behavior of topological defect–defect correlation functions in two-dimensional systems driven out of equilibrium to regimes where they exhibit "defect chaos". Using the topological nature of the defects, we show that these defect–defect correlations cannot decay as slowly as predicted by generic scale invariance. We also provide numerical calculations that yield defect–defect correlation functions in the defect turbulence regime of the two-dimensional, anisotropic complex Ginzburg–Landau equation. These numerical results, which test the specific regime of broken square symmetry, do not appear to decay as slowly as predicted by the ideas of generic scale invariance. These results are in agreement with the analytical predictions.

PACS: 05.45.+b; 47.20.Tg
Keywords: Generic scale invariance; Topological defects; Complex Ginzburg–Landau equation

1. Introduction

In equilibrium systems, spatial correlations typically decay exponentially, with the decay length scale set by the correlation length ξ. A system will exhibit slow algebraic decay of spatial correlations only by having its parameters adjusted to a critical point. For externally driven nonequilibrium systems the situation can be quite different: in a system with a conservation law and external noise, spatial correlation functions can decay algebraically. It has been suggested [1–5] that this algebraic decay is expected to occur for a broad range of conditions (tuning parameters to a critical point is not required), and such behavior has been called "generic scale invariance". It has also been argued for various nonlinear deterministic equations, such as the Kuramoto–Sivashinsky (KS) equation, that the external noise used for the predictions of generic scale invariance can be replaced by noise originating from the chaotic behavior of the system [6–12]. The predictions of generic scale invariance have been tested in molecular fluid systems such as toluene subject to temperature gradients. These experiments, which use small-angle Rayleigh

* Corresponding author.

PII S0167-2789(96)00127-3

scattering to measure correlations between density fluctuations in the fluid, do show evidence of long range behavior in these correlations [13,14]. A review of generic scale invariance and the experimental tests in fluids is given in [15].

Driven, spatially extended systems with many interacting degrees of freedom often show nonrelaxational behavior, called spatiotemporal chaos [16], in which chaotic fluctuations occur in space as well as in time. Typically, spatiotemporal chaos appears in nonequilibrium pattern-forming systems slightly above their threshold of instability [17]. Many of these systems exhibit a particular kind of spatiotemporal chaos dominated by the continual creation, annihilation, and interaction of defects. This behavior has been called "weak turbulence", "defect chaos", and "defect turbulence". (This is to be distinguished from fully developed turbulence, which typically occurs for increasing driving but fixed system size L, while spatiotemporal chaos occurs for fixed large driving but increasing L.) The study of spatiotemporal chaos has been advanced by the development of experimental systems which are precisely controlled and have a large aspect ratio. These systems, including Rayleigh–Bénard convection [18–21], electrohydrodynamic convection in liquid crystals [22–26], capillary ripples [27], cardiac tissue [28], chemical reactions [29], and wide aperture lasers [30,31], can exhibit defect-turbulent behavior. Such systems appear to have large statistically homogeneous regions relatively free from boundary effects, and we may hope to use a statistical description of the spatiotemporal chaotic states, borrowing concepts from equilibrium statistical mechanics. We would like to find simple reduced descriptions, emphasizing the collective behavior of many chaotic degrees of freedom, analogous to the reduced long-wavelength description provided by thermodynamics and hydrodynamics for equilibrium systems [8,9,32–35].

In this paper we will focus our attention on the question of the applicability of generic scale invariance to the dynamics of topological defects in systems that can be described by nonrelaxational, complex order parameter equations. In analogy to the mapping of the deterministic Kuramoto–Sivashinsky equation to the stochastic Kardar–Parisi–Zhang equation [12], we assume that the defect density is a fluctuating field with noise, which we speculate is chaotic in nature because the fluctuations in the underlying field are chaotic. Based on general arguments, we show that power laws as predicted by generic scale invariance cannot be observed. To test these ideas we consider the coherent topological structures known as defects or spirals or vortices in a system that exhibits spatiotemporal chaos: the complex Ginzburg–Landau equation [36–40]. This equation describes the slowly varying amplitude and phase in an extended system which undergoes a supercritical Hopf bifurcation to an oscillating and spatially uniform or oscillatory and spatially periodic state. The equation exhibits many interesting phenomena, but we will restrict our investigation to the portion of the Benjamin–Feir unstable regime [41–44], in which topological defects occur in the context of spatiotemporal chaos.

This paper is organized as follows. In Section 2 we briefly describe the ideas behind generic scale invariance. Constraints on the behavior of topological defects due to their topological nature are discussed in Section 3. In Section 4 we discuss briefly the complex Ginzburg–Landau equation and its topological defects. The predictions of generic scale invariance, as well as that from the constraints, are compared with numerical results in Section 5. Finally, we present our conclusions in Section 6.

2. Generic scale invariance

Generic scale invariance [1–5] is expected to occur in nonequilibrium systems described by a stochastic partial differential equation:

$$\partial_t \rho(\boldsymbol{r}, t) = \Gamma\{\rho(\boldsymbol{r}, t)\} + \eta(\boldsymbol{r}, t), \tag{1}$$

where Γ is a general conserving operator on the field ρ, such as $\Gamma_0\nabla^2 + \Gamma_1(\nabla^2)^2 + \Gamma_{2x}\partial_x^4 + \Gamma_{2y}\partial_y^4$. This operator can also contain nonlinear terms (e.g. $\nabla \cdot [(\nabla^2\rho)(\nabla\rho)]$). The stochastic noise term η is defined by:

$$\langle \eta(\boldsymbol{r}, t)\rangle = 0, \tag{2}$$

$$\langle \eta(\boldsymbol{r}, t)\eta(\boldsymbol{r}', t')\rangle = D\delta(\boldsymbol{r} - \boldsymbol{r}')\delta(t - t'), \tag{3}$$

where D must be composed of differential operators for a strictly conserved order parameter such as one describing topological defects. Note that Eq. (1) assumes that we can write down a local equation of motion for the order parameter ρ.

For nonlinear, nonequilibrium system with conserving noise (e.g. $D = D_1\nabla^2$), equations (1– 3) can lead to generic scale invariance, or scale invariance in the absence of any parameter tuning [2]. If such a system is isotropic, then one obtains exponential decays in the two-point correlation function $G_\rho(\boldsymbol{r}) \equiv \langle \rho(\boldsymbol{r})\rho(\boldsymbol{0})\rangle$, with power law decays (*i. e.* scale invariance) occuring in higher order correlation functions. In anisotropic systems, $G_\rho(\boldsymbol{r})$ does show algebraic decay. For systems with cubic symmetry, $G_\rho(\boldsymbol{r}) \sim 1/r^{d+2}$ for large r, where d is the dimension of the system. For systems which break cubic symmetry, $G_\rho(\boldsymbol{r}) \sim 1/r^d$. We will limit our study the last regime, a two-dimensional system with broken square symmetry, where generic scale invariance predicts that

$$G_\rho^{\text{generic}}(\boldsymbol{r}) = \langle \rho(\boldsymbol{r})\rho(\boldsymbol{0})\rangle \sim 1/r^2 \tag{4}$$

for large r [2].

It has been shown [10,11,45,46] that some extended deterministic chaotic systems also exhibit algebraic decay of the two-point correlation function of the order parameter field. In at least one of these examples [10], the chaotic fluctuations appear to play the same role as stochastic noise in the equations describing the evolution of the order parameter. In other words, the conserving noise term in Eq. (1) can represent the effect of the chaotic fluctuations. There is also evidence from the mapping of the Kuramoto–Sivashinsky equation to the Kardar–Parisi–Zhang equation [6,7,12,47,48] and from coupled map lattices [10] that this identification of spatiotemporal chaotic fluctuations with stochastic noise is not unreasonable.

The predictions of generic scale invariance depend upon showing that nonlinearities in the equations are irrelevant in a renormalization group sense. This means that as the scale on which the system is examined grows, the importance of the nonlinearities in the dynamics at the larger scale is less important. This analysis is usually carried out in a perturbative manner, where the strength of the nonlinear term is the small expansion parameter. Systems with topological defects have been notoriously difficult to treat in a perturbative manner. An example of this difficulty is the Kosterlitz–Thouless transition [49]. With this difficulty in mind, we will still proceed to consider generic scale invariance for nonequilibrium, nonlinear systems with topological defects, first presenting results that depend only on the topological nature of the defects.

3. Topological constraints

We wish to define an order parameter $\rho(\boldsymbol{r})$ that is a measure of the density of topological defects, and that also takes into consideration the topological nature of these defects. If we know the locations $\boldsymbol{r}_i$ of the defects, then we can define an order parameter

$$\rho(\boldsymbol{r}) = \sum_i q_i\, \delta\,(\boldsymbol{r} - \boldsymbol{r}_i)\,, \tag{5}$$

where q_i represents the topological "charge" of the defect. Topological defects can come in several varieties. For example, in the two-dimensional complex Ginzburg–Landau equation there are two types of defects, with charge

(or winding number) $+1$ or -1. These defects occur where the phase of the underlying complex field A changes by $+2\pi$ or -2π as we follow a path counterclockwise about a point. If we write the complex field as a modulus and phase

$$A = |A|e^{i\varphi}, \tag{6}$$

then we can write down a concrete expression for ρ without needing to know the location of the topological defects:

$$\rho(\boldsymbol{r}) = \lim_{R\to 0} \frac{1}{\pi R^2} \oint_C \frac{\nabla\varphi(\boldsymbol{r}') \cdot d\boldsymbol{s}'}{2\pi}, \tag{7}$$

where C represents a circle of radius R about the point r. The connection between the two definitions can be seen by considering the fundamental definition of the δ-function [50]. Note that for the complex Ginzburg–Landau equation, the topological defects occur where lines of $\mathrm{Re}[A] = 0$ and $\mathrm{Im}[A] = 0$ cross (i.e. $A = 0$), and the presence of such topological defects can be detected far away due to discontinuities in the phase φ.

The excess order parameter in a region is defined as

$$\delta\rho_L \equiv \left| \int_{r\in C(L)} (\rho(\boldsymbol{r} + \boldsymbol{r}_0) - \rho_0)\, d\boldsymbol{r} \right|, \tag{8}$$

where $C(L)$ represents a circle of radius L about a point $\mathbf{r}_0$, which we take as $\boldsymbol{r}_0 = \mathbf{0}$ due to translational invariance, and where ρ_0 is the average order parameter. (In the case of topological defects ρ_0 is 0.) Note that we are performing the integration over the entire surface of the circle, not just along the perimeter. If ρ represented nontopological objects, the excess order parameter would be constrained: $\delta\rho_L \leq a_1 L^2$, where a_1 is some numerical constant. In other words, for a nontopological order parameter the individual objects occupy fixed areas. For topological defects of the type we are studying, the situation is different; here, $\delta\rho_L \leq a_2 L$, where a_2 is again some numerical constant.

To derive this constraint, consider a box of dimension $L \times L$ with topological defects inside. By their very nature, any excess topological defects in this box are detectable simply by traversing the perimeter of the box. In fact, an alternative (and equivalent) definition of the excess order parameter in an $L \times L$ region is

$$\delta\rho_L = \left| \oint_{L\times L} \frac{\nabla\varphi(\boldsymbol{r}') \cdot d\boldsymbol{s}'}{2\pi} \right|. \tag{9}$$

This measurement is a local measurement on the perimeter, because each topological defect has some characteristic "arm" which must pass through the boundary of the box. In the complex Ginzburg–Landau equation, these are lines of discontinuity in the phase φ for the complex field A. Other examples are spiral arms of the defects in Rayleigh–Bénard convection and extra rows of atoms for dislocations in crystals. These arms take up some minimal size l of the perimeter. If the arms were forced closer than this minimal size, the gradient $\nabla\varphi$ would increase to a value that is not sustainable in any physical system.

For the complex Ginzburg–Landau equation, one can determine the number of $+2\pi$ phase jumps and the number of -2π phase jumps along the perimeter. The difference between these two numbers then gives the excess number of defects inside the perimeter. When a region contains the maximum excess number of defects allowed, each of these 2π phase jumps takes up the minimal size $l \sim 1/[\nabla\varphi]_{\max}$ of the perimeter of the region. This occurs when the phase jumps are squeezed as close as physically possible on the perimeter. This minimal size is the same no matter what size region is being considered.

For the $L \times L$ box, the maximum excess is equal to the perimeter of the box divided by l. For a box with twice the perimeter, the linear size for the phase jumps when squeezed as close as possible is still l, since this is determined by local structure on the perimeter of the box. However, the perimeter is twice as large, so we can have twice as many jumps squeezed along the perimeter, and twice as many excess defects inside the region. This doubling of the maximum excess defects with a doubling of the perimeter implies that the maximum excess of topological defects $\mathrm{Max}(L) \propto L$, or $\delta\rho_L \leq a_2 L$.

If we assume that the correlation function $G_\rho(\boldsymbol{r})$ decays at the same asymptotic rate independent of the direction of $\boldsymbol{r}$, i.e. $G_\rho(\boldsymbol{r}) \sim f(\theta)g(r)$ where $g(r) \sim 1/r^\alpha$ for large r, then with the constraint on topological objects we can show for two dimensions that α must be greater than 2, which contradicts the prediction of generic scale invariance. This result also requires that $\int_0^{2\pi} f(\theta)\,\mathrm{d}\theta \neq 0$, which we expect to be true except for special cases; we discuss this point further in Section 3.1. A correlation function satisfying both assumptions occurs, for example, in studies of nonequilibrium conservative anisotropic lattice gases [51,52]. To show that $\alpha > 2$, we use the inequality $\delta\rho_L \leq aL$. Squaring this relation yields

$$\int_{r\in C(L)} \int_{r'\in C(L)} \mathrm{d}\boldsymbol{r}\,\mathrm{d}\boldsymbol{r}'\rho(\boldsymbol{r},t)\rho(\boldsymbol{r}',t) \leq a^2L^2. \tag{10}$$

Now we average over the noise (or over space and time, depending on whether the average is for a stochastic equation or for a deterministic chaotic equation). For a stochastic average, we mean that an average $\langle f\rangle$ is given by

$$\langle f(\eta)\rangle = \int \mathrm{d}\eta P(\eta) f(\eta), \tag{11}$$

where η is a stochastic noise and $P(\eta)$ is the measure of the probability for this stochastic noise (for white noise, $P(\eta)$ is a Gaussian). A similar definition can be given for the case where we average over space and time in a chaotic system.

Using this gives the constraint equation

$$\langle \delta\rho_L^2\rangle \leq a^2L^2. \tag{12}$$

The averaging process can be moved inside the integrals in $\delta\rho_L^2$, and then we can make the replacement

$$\langle \rho(\boldsymbol{r},t)\rho(\boldsymbol{r}',t)\rangle \to G_\rho(\boldsymbol{r}-\boldsymbol{r}'). \tag{13}$$

This yields our final constraint equation

$$\int_{r\in C(L)} \int_{r'\in C(L)} \mathrm{d}\boldsymbol{r}\,\mathrm{d}\boldsymbol{r}' G_\rho(\boldsymbol{r}-\boldsymbol{r}') \leq a^2L^2. \tag{14}$$

We now assume that we can write $G_\rho(\boldsymbol{r}) = f(\theta)g(r)$ where θ is the angle for $\boldsymbol{r}$ and $r = |\boldsymbol{r}|$. Strictly speaking, this assumption is only necessary for large r. Given that G_ρ takes this form, we can write

$$\int_{r\in C(L)} \int_{r'\in C(L)} \mathrm{d}\boldsymbol{r}\,\mathrm{d}\boldsymbol{r}' G_\rho(\boldsymbol{r}-\boldsymbol{r}') = \frac{1}{2\pi}\int_0^{2\pi} f(\theta)\,\mathrm{d}\theta \int_0^{2L} g(R)w(R)\,\mathrm{d}R, \tag{15}$$

where $w(R)$ is given by

$$w(R) = \int_{r\in C(L)} \int_{r'\in C(L)} S(R)\delta(\boldsymbol{r}-\boldsymbol{r}'-\boldsymbol{R})\,\mathrm{d}\boldsymbol{r}\,\mathrm{d}\boldsymbol{r}' \tag{16}$$

with $S(R) = 2\pi R$ the perimeter of a circle of radius R. We further assume that $\int_0^{2\pi} f(\theta)\,\mathrm{d}\theta \neq 0$. We can calculate a closed form expression for $w(R)$ using the definition of $\delta(\boldsymbol{x})$:

$$\delta(\boldsymbol{x}) \equiv \frac{1}{(2\pi)^2} \int_{-\infty}^{\infty} \mathrm{d}\boldsymbol{k} \mathrm{e}^{\mathrm{i}\boldsymbol{k}\cdot\mathbf{x}}. \tag{17}$$

Substituting this into Eq. (16) gives

$$w(R) = \frac{2\pi R}{(2\pi)^2} \int_{-\infty}^{\infty} \mathrm{d}\boldsymbol{k} \mathrm{e}^{-\mathrm{i}\boldsymbol{k}\cdot\boldsymbol{R}} \int_{\boldsymbol{r}\in C(L)} \mathrm{d}\boldsymbol{r} \mathrm{e}^{\mathrm{i}\boldsymbol{k}\cdot\boldsymbol{r}} \int_{\boldsymbol{r}'\in C(L)} \mathrm{d}\boldsymbol{r}' \mathrm{e}^{-\mathrm{i}\boldsymbol{k}\cdot\boldsymbol{r}'}. \tag{18}$$

The integrals over $C(L)$ are given by

$$\int_{\boldsymbol{r}\in C(L)} \mathrm{d}\boldsymbol{r} \mathrm{e}^{\mathrm{i}\boldsymbol{k}\cdot\boldsymbol{r}} = \int_0^L \int_0^{2\pi} r\,\mathrm{d}r\,\mathrm{d}\theta \mathrm{e}^{\mathrm{i}kr\cos\theta} = \frac{2\pi L}{k} J_1(kL), \tag{19}$$

where J_1 is the first order Bessel function. Substituting this result in Eq. (18), we obtain

$$w(R) = 2\pi RL^2 \int_{-\infty}^{\infty} \mathrm{d}\boldsymbol{k} \mathrm{e}^{-\mathrm{i}\boldsymbol{k}\cdot\boldsymbol{R}} \frac{J_1^2(kL)}{k^2} = 4\pi^2 RL^2 \int_0^{\infty} \frac{\mathrm{d}k}{k} J_0\left(k\frac{R}{L}\right) J_1^2(k). \tag{20}$$

Performing this last integral [53] gives

$$w(R) = 4\pi RL^2 \left[\cos^{-1}\left(\frac{R}{2L}\right) - \frac{R}{2L}\sqrt{1-\left(\frac{R}{2L}\right)^2}\right]. \tag{21}$$

We can check this by noting that $\int_0^{2L} w(R)\,\mathrm{d}R = \pi^2 L^4$, which is just $\left(\int_{\boldsymbol{r}\in C(L)} \mathrm{d}\boldsymbol{r}\right)^2$.

Next, we apply $w(R)$ to the problem at hand. Suppose that $g(R)$ in Eq. (15) exhibits its asymptotic behavior outside of some $R = r_{\min}$, $g(R) \sim R^{-\alpha}$ for $R > r_{\min}$ and also that $L \gg r_{\min}$. Splitting the integral into two parts yields

$$\int_0^{2L} g(R)w(R)\,\mathrm{d}R = \left(\int_0^{r_{\min}} + \int_{r_{\min}}^{2L}\right) g(R)w(R)\,\mathrm{d}R. \tag{22}$$

We consider each of these terms separately. The first term can be bounded as follows:

$$\left|\int_0^{r_{\min}} g(R)w(R)\,\mathrm{d}R\right| \leq |g_{\max}| \int_0^{r_{\min}} w(R)\,\mathrm{d}R. \tag{23}$$

We can evaluate the integral of $w(R)$ exactly. To do this, we set $\xi = R/2L$. The integral is then

$$4\pi L^2(4L^2) \int_0^{r_{\min}/2L} \left[\xi\cos^{-1}\xi - \xi^2\sqrt{1-\xi^2}\right] \mathrm{d}\xi. \tag{24}$$

Performing the integral (with $\xi_{\min} = r_{\min}/2L$) gives

$$4\pi L^2(4L^2)\left[\tfrac{1}{4}\xi_{\min}(1-\xi_{\min})^{3/2} - \tfrac{3}{8}\xi_{\min}\sqrt{1-\xi_{\min}^2} + \tfrac{1}{8}\sin^{-1}\xi_{\min} + \tfrac{1}{2}\xi_{\min}^2\cos^{-1}\xi_{\min}\right]. \tag{25}$$

Expanding this about $\xi_{\min} = 0$ gives

$$\left|\int_0^{r_{\min}} g(R)w(R)\,\mathrm{d}R\right| \leq \pi^2 r_{\min}^2\,|g_{\max}|\,L^2 + \mathrm{O}(L) \tag{26}$$

for large L.

For the second integral in Eq. (22), we assume that $g(R) = g_0 R^{-\alpha}$. Substituting Eq. (21) for $w(R)$ and again making the change of variable $\xi = R/2L$, the integral can be written as

$$4\pi L^2(2L)^{2-\alpha} g_0 \int_{r_{\min}/2L}^{1} \left[\xi^{1-\alpha}\cos^{-1}\xi - \xi^{2-\alpha}\sqrt{1-\xi^2}\right]\mathrm{d}\xi. \tag{27}$$

In this integral, there are no singularities due to the upper limit of 1, since the integrand is analytic there for all α. However, at the lower limit, as $\xi \to 0$ ($L \to \infty$), there can be divergences, depending on the value of α. The integrand, upon expansion about $\xi = 0$, becomes

$$\xi^{-\alpha}\left[\tfrac{1}{2}\pi\xi - 2\xi^2 + \mathrm{O}(\xi^4)\right]. \tag{28}$$

Now, suppose that $\alpha < 2$. Then the integrand has an integrable singularity at $\xi = 0$, and as $L \to \infty$ we obtain some constant plus correction terms that die away for large L. For $\alpha = 2$ we get a logarithmic divergence, and for $\alpha > 2$ a diverging term $L^{\alpha-2}$ which exactly cancels the $L^{2-\alpha}$ in front of Eq. (27).

The leading order behavior of $\langle \delta\rho_L^2 \rangle$ is then

$$\alpha < 2:\ \langle \delta\rho_L^2 \rangle \sim L^2 L^{2-\alpha}, \quad \alpha = 2:\ \langle \delta\rho_L^2 \rangle \sim L^2 \log(L), \quad \alpha > 2:\ \langle \delta\rho_L^2 \rangle \sim L^2. \tag{29}$$

Recall that the prediction from generic scale invariance is $\alpha = 2$ (see Eq. (4)). However, this case violates the constraint for topological defects given by Eq. (12). Within our assumptions, this result means that for topological objects the results of generic scale invariance cannot hold. In fact, what we have provided is a bound on α. For topological objects, the decay of $G_\rho(r)$ must be strictly faster than r^{-2} (i.e. α must be greater than 2). The simple geometric nature of topological objects prevents them from having correlation functions that decay as certain power laws. (A decay of $1/(r^2(\log r)^\beta)$ for $\beta > 1$ does satisfy our bounds on $\langle \delta\rho_L^2 \rangle$, but is not consistent with the predictions of generic scale invariance.)

In our analysis we have only considered the largest possible fluctuations. We expect these fluctuations to be rare, and hence expect a faster decay than the bound we provide. As an analogy, for nontopological objects the analysis presented here would predict that the correlation function can be at most a constant for large r; in practice, systems like spins or atoms have connected correlation functions that decay to zero, either as power laws or as exponentials. However, it is often true that inequalities in physics are saturated, especially in relationships between critical exponents for phase transitions. This could be the case here, but numerically for the example of the complex Ginzburg–Landau equation it appears that we do not saturate this bound, as shown in Section 5.

3.1. Splitting the correlation function

We now consider the splitting of the correlation function into angular and radial factors, which is important for the analysis given above. While we cannot explicitly show that such a splitting occurs for the topological defects, we can demonstrate a splitting in the context of generic scale invariance. We start with the general result for the correlation function [2]

$$G(\boldsymbol{r}) = \int \mathrm{d}\boldsymbol{k} \mathrm{e}^{\mathrm{i}\boldsymbol{k}\cdot\boldsymbol{x}} \frac{D(\boldsymbol{k})}{\Gamma(\boldsymbol{k})}, \tag{30}$$

where D and Γ are defined in Eqs. (1) and (3). Then we define the angular average

$$G(r) = \frac{1}{2\pi} \int_0^{2\pi} G(\boldsymbol{r})\, \mathrm{d}\theta, \tag{31}$$

where $\boldsymbol{r} = (r\cos\theta, r\sin\theta)$. Using these two equations gives

$$G(r) = \frac{1}{2\pi} \int_0^{2\pi} \mathrm{d}\theta \int \mathrm{d}\boldsymbol{k} \frac{D(\boldsymbol{k})}{\Gamma(\boldsymbol{k})} \mathrm{e}^{\mathrm{i}(k_x r\cos\theta + k_y r\sin\theta)}. \tag{32}$$

Performing the θ integral yields

$$G(r) = \int \mathrm{d}\boldsymbol{k} \frac{D(\boldsymbol{k})}{\Gamma(\boldsymbol{k})} J_0\left(r\sqrt{k_x^2 + k_y^2}\right), \tag{33}$$

where J_0 is the zeroth order Bessel function. This expression is not in general zero for arbitrary r.

We can also give a concrete expression, in a particular limit, for $G(r)$. We begin with specific expressions for $D(\boldsymbol{k})$ and $\Gamma(\boldsymbol{k})$, and ignore questions of convergence of the integrals for large k, since in physical systems there will be higher order terms that guarantee convergence. Here we choose the specific (linearized) forms:

$$D(\boldsymbol{k}) = D_x k_x^2 + D_y k_y^2, \qquad \Gamma(\boldsymbol{k}) = \Gamma_x k_x^2 + \Gamma_y k_y^2. \tag{34}$$

Using these forms Eq. (30) becomes

$$G(\boldsymbol{r}) = \int_{-\infty}^{\infty} \int_{-\infty}^{\infty} \mathrm{d}k_x\, \mathrm{d}k_y \mathrm{e}^{\mathrm{i}(k_x x + k_y y)} \left(\frac{D_x k_x^2 + D_y k_y^2}{\Gamma_x k_x^2 + \Gamma_y k_y^2}\right). \tag{35}$$

The k_x integral can be performed as a contour integral; the expression has poles at $k_x = \pm\mathrm{i}\sqrt{\Gamma_y/\Gamma_x}\, k_y \equiv \pm\mathrm{i}\gamma k_y$. We assume for ease of calculation the $x > 0$ and $y > 0$; the results are the same for other cases. When $k_y > 0$, we close the contour in the upper half of the complex k_x plane, enclosing the pole at $\mathrm{i}\gamma k_y$. For $k_y < 0$ we enclose the pole at $-\mathrm{i}\gamma k_y$. The integral then becomes $2\pi\mathrm{i}$ times the residue at $k_x = \mathrm{i}\gamma k_y$. Then we obtain

$$G(\boldsymbol{r}) = \frac{\pi}{\Gamma_x \gamma}(D_y - D_x\gamma^2) \left(\int_0^{\infty} \mathrm{d}k_y\, k_y \mathrm{e}^{-k_y(\gamma x - \mathrm{i}y)} + \int_{-\infty}^{0} \mathrm{d}k_y\, k_y \mathrm{e}^{-k_y(-\gamma x - \mathrm{i}y)} \right). \tag{36}$$

By performing the k_y integrals we obtain (using $x = r\cos\theta$ and $y = r\sin\theta$)

$$G(\boldsymbol{r}) = \frac{2\pi(D_y\Gamma_x - D_x\Gamma_y)}{\sqrt{\Gamma_x\Gamma_y}} \left(\frac{\Gamma_y \cos^2\theta - \Gamma_x \sin^2\theta}{(\Gamma_y \cos^2\theta + \Gamma_x \sin^2\theta)^2}\right) \frac{1}{r^2}. \tag{37}$$

Note that our results are for the case $\Gamma_x \neq \Gamma_y$, so we have for this simple example the result that the angular average is not zero. Also, Eq. (37) is explicitly split into a radial and angular component.

4. The complex Ginzburg–Landau equation

Perturbative analyses of microscopic equations for various pattern-forming systems yield partial differential equations often referred to as "amplitude" or "envelope" equations. Because these equations typically describe periodic patterns, they are complex (i.e. the fields have two components). Considered in their own right as model dynamical systems which do not necessarily describe any real physical system, these equations are referred to as Ginzburg–Landau models. Many hard problems, such as the existence and interaction of defects and coherent structures, or the appearance of chaos, can be profitably addressed in the simple framework provided by these equations. However, these equations provide a quantitative description of real experiments only in the vicinity of the transition threshold for a pattern. Far from threshold, only the phase of the complex field survives as a slow degree of freedom, since it describes a symmetry of the system. The amplitude of the complex field only becomes slow near threshold; far away it is just one of the many fast degrees of freedom.

We wish to consider spatiotemporal chaos and topological defects in an equation that has been used both as an "amplitude equation" in the sense discussed above as well as a model equation to study generic features of spatially extended nonlinear dynamical systems. We are using the equation as a model equation for spatiotemporal chaos. The complex Ginzburg–Landau equation we consider is given by

$$\partial_t A = A - (1 + \mathrm{i}c)|A|^2 A + (1 + \mathrm{i}b_x)\partial_x^2 A + (1 + \mathrm{i}b_y)\partial_y^2 A, \tag{38}$$

where A is a complex field in two dimensions [54]. This equation can have topological defect solutions where $A = 0$ (both Re[A] and Im[A] are zero) [36–39,55–59]. These defects can occur either in static arrangements or in dynamic ones. The dynamic states can have defects moving in a regular fashion (for example, all defects drifting in one direction [57]) or they can exhibit defect turbulence, where defects are continuously nucleated and annihilated in pairs and are moving about in a chaotic, nonregular fashion [36]. We wish to focus on the latter case. To do this, we choose parameters so the system is far enough into the Benjamin–Feir unstable regime [41–44] that it exhibits defect chaos. Note that this Benjamin–Feir regime occurs when $1 + b_\alpha c < 0$. In this region of parameter space, all plane-wave solutions of the complex Ginzburg–Landau equation are unstable (when considered in a linear stability analysis). For comparison with the ideas of generic scale invariance [1–5], we will focus on the anisotropic case $b_x \neq b_y$. (Note that in this regime the qualitative behavior of the solutions of the complex Ginzburg–Landau equation did not change significantly from results obtained in the isotropic case.)

As discussed in Section 3, the topological defects in the complex Ginzburg–Landau equation come in two types. A defect with a phase jump of 2π has a topological charge of $+1$, while one with a jump of -2π has a topological charge of -1. This is analogous to the right-handed and left-handed single-armed spirals in Belousov–Zhabotinskii reactions [60], for example. If we let $\rho_+(\boldsymbol{r})$ equal the density of $+1$ defects and $\rho_-(\boldsymbol{r})$ equal the density of -1 defects, we can define a "topological" order parameter, $\rho(\boldsymbol{r}) \equiv \rho_+(\boldsymbol{r}) - \rho_-(\boldsymbol{r})$, which is just the density of the defects weighted by their topological charge. This is equivalent to the order parameter ρ considered previously. This order parameter is conserved in a system with periodic boundary conditions, or in a system where the amplitude is held at a finite nonzero value on the boundaries (usually termed boundary forcing in the literature). The latter situation is typical in an experimental system. In both cases, $\int_V \rho(\boldsymbol{r})\mathrm{d}\boldsymbol{r} = 0$, as defects can only be created or destroyed in $+/-$ pairs. We will focus on the topological order parameter $\rho(\boldsymbol{r})$ by comparing simulations of the complex Ginzburg–Landau equation to the predictions of generic scale invariance.

Although the time evolution of ensembles of defects is very complicated, considerable progress has been made in the study of the dynamics of isolated or weakly interacting defects. Defects are isolated singularities in the phase equation (for the phase of A), but are smooth solutions of the full equations. It is an attractive idea to imagine a description in terms of coupled dynamics of phase and defect degrees of freedom. Progress on this idea has been made in the case of Rayleigh–Bénard convection [35,61,62] and the Kuramoto–Sivaskinsky equation [34]; for a review of the situation in the two-dimensional complex Ginzburg–Landau equation see [17, pp. 920–922].

The complex Ginzburg–Landau equation appears to satisfy the criterion for generic scale invariance; it shows nonequilibrium behavior since it cannot be derived from an underlying potential (i.e. it is nonrelaxational), and in a system with periodic boundary conditions, the topological order parameter $\rho(\boldsymbol{r})$ is conserved. We conjecture that the chaotic noise in our system plays the role of the stochastic noise described in Eqs. (1– 3). This mapping of chaotic fluctuations to stochastic noise is a hypothesis, although there is growing evidence that deterministic chaotic fluctuations can produce results for asymptotic correlations similar to that seen in systems with Gaussian noise [6–12]. Finally, we also note that generic scale invariance requires short-ranged interactions. There is some evidence that this occurs for the defects in the complex Ginzburg–Landau equation [63,64], but collective effects might be important.

5. Numerical results for the defects

We have performed numerical simulations in the defect–turbulent regime of the complex Ginzburg–Landau equation. These simulations, in addition to providing a comparison with the results in Section 3, demonstrate the types of techniques necessary to extract defect–defect correlation functions from experiments and theory.

For the simulations, we have numerically solved Eq. (38) with periodic boundary conditions using a Fourier collocation (or pseudospectral) code [65,66]. Our original code was obtained from J. Lega, L. Gil, and P. Coullet (see Ref. [36–39,67]), and is now used as the basis for simulations by several groups.

The system is 240×240 in real space, with 360 Fourier modes in each direction. The time step used was $\delta t = 0.02$. We use the parameter values $b_x = -0.75$, $b_y = -3.0$, and $c = 1.5$, . With these parameters, our choice of time step and number of Fourier modes ensures that our discretized numerical simulation results accurately represent the solution for the continuum partial differential equation (38). We have performed simulations with smaller time steps and larger numbers of Fourier modes, and see no significant difference from the original simulations. The parameters b_x, b_y, and c were chosen in the Benjamin–Feir unstable regime [41–44] to give a reasonable number of defects while still allowing the system to be simulated with a relatively small number of Fourier modes and a fairly large time step.

We start our systems with two different types of initial conditions. One initial condition is to seed the system with two oppositely charged topological defects. The other is to begin with random initial conditions (for instance a uniform distribution between -0.1 and 0.1 for the field A). After starting, we have to wait for the system to "equilibrate" to a steady-state condition (meaning fluctuations about an average number of defects). This takes, for our typical parameters, on the order of 5000 time steps with the step size of $\delta t = 0.02$. This steady-state condition is a statistically stationary state, where averages depend only on differences of space and time coordinates. The numerical results for the defects do not depend upon which initial condition is chosen.

We note that the defects do not form bound pairs. When a pair is created, the defects tend to move apart, and when they eventually annihilate, they usually do so with a defect other than their initial partner. This illustrates that the system is not in a Kosterlitz–Thouless bound pair phase [49]. Fig. 1 is a snapshot of part of the simulated system, showing the two types of defects, and lines of $\mathrm{Re}[A] = 0$ and $\mathrm{Im}[A] = 0$.

Topological defects have been studied in systems undergoing phase ordering. In these systems (an example is the XY model) the existence of an underlying Hamiltonian allows analytic progress to be made [68,69] in the form of

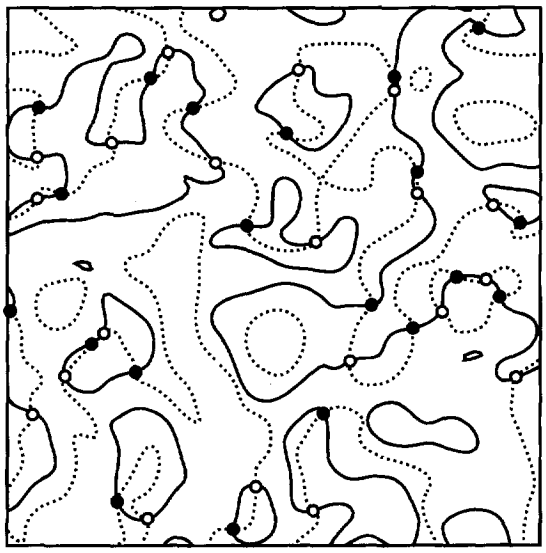

Fig. 1. Snapshot of a 70 × 70 region. This is approximately $\frac{1}{12}$ of the total area of the simulation. The solid lines are Re[A] = 0 and the dashed lines are Im[A] = 0. Filled circles (•) are vortices with topological charge +1 and the open circles (○) have charge −1. The typical distance between defects is 10. This picture is for $b_x = -0.75$, $b_y = -3.0$, and $c = 1.5$.

perturbation expansions. Some numerical work has also been performed on these systems [70]. For our system, the numerical results are key as we cannot form perturbation expansions due to the lack of an underlying Hamiltonian.

To find the defects in the system, we examine the change in the phase of A as each plaquette (or square unit cell) on our lattice in real space is traversed counterclockwise. To do this, we examine the phase $\varphi(\boldsymbol{x}, t) \equiv \tan^{-1}(\text{Im } A(\boldsymbol{x}, t)/\text{Re } A(\boldsymbol{x}, t))$ as we go around a plaquette on the lattice and sum up the phase differences between the four points in the plaquette. A change of 0 signifies that the plaquette does not contain a defect, while changes of $\pm 2\pi$ reveal that a defect exists in the plaquette. We can actually speed up the defect finding process: If all four sites in the plaquette have the same sign of Re[A] or of Im[A], then the plaquette cannot contain a defect. More complicated situations can also be handled, such as where one corner of the plaquette is of a different sign from the other three corners for Re[A], while the opposite corner from the original one is of a different sign from the other three corners for Im[A]. In this case, the plaquette cannot contain a defect. These considerations avoid the costly calculation of $\tan^{-1}$, and can be used for a large fraction of the plaquettes in the lattice.

Once we have found the defects, we can calculate $n(t)$, the total number of defects in the system, and $G_\rho(\boldsymbol{r})$. To do the averaging, we have run for 750 000 time steps. We only sample $G_\rho(\boldsymbol{r})$ and $n(t)$ every 10 time steps, because adjacent time steps are not statistically independent. We have calculated that $\langle n(t)n(0)\rangle - \langle n\rangle^2 \sim \mathrm{e}^{-t/\tau}$, with $\tau \sim 115$ time steps. It has been predicted [38] that the probability of finding a particular value of n in the system is given by $P(n) \sim \mathrm{e}^{-(n-\langle n\rangle)^2/2\langle n\rangle}$. We have calculated the various moments of our distribution $P(n)$, and we find $\langle n\rangle = 422.8 \pm 0.3$, $\sigma^2 = 397 \pm 30$, as well as a skewness of 0.014 and a kurtosis of −0.026, which is in good agreement with the results in reference [38]. In Fig. 2, we present a plot of the results for $P(n)$ together with the fitted Gaussian. The agreement is excellent.

In order to test the idea of topological constraints in the complex Ginzburg–Landau equation, we have examined the quantity $\delta\rho_L$, as defined by Eq. (8). As argued in Section 3, the inequality $\delta\rho_L \leq a_2 L$ should hold for topological defects. We have calculated $\delta\rho_L/L$, averaged over 138 different snapshots of our system. The results are given in Fig. 3. From this figure we see that $\langle\delta\rho_L\rangle/L$ is decaying as a functions of L, illustrating that the inequality is satisfied. In fact, from these data our best estimate is that $\langle\delta\rho_L\rangle \sim L^\nu$, with $\nu = 0.5 \pm 0.1$. This result is what we would expect

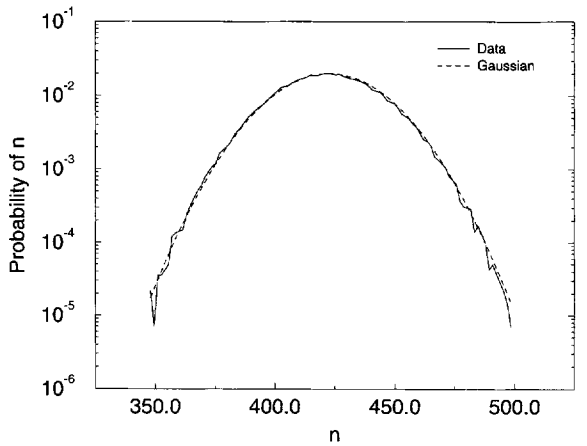

Fig. 2. Prob(n). This was obtained from a time series of length 70 000 time steps. This is for a system of size $L_x = L_y = 240$ with 360 Fourier modes in each direction. The parameter values are $b_x = -0.75$, $b_y = -3.0$ and $c = 1.5$. The dashed line is the exponential with mean $\mu = 422.8$ and $\sigma^2 = 397$.

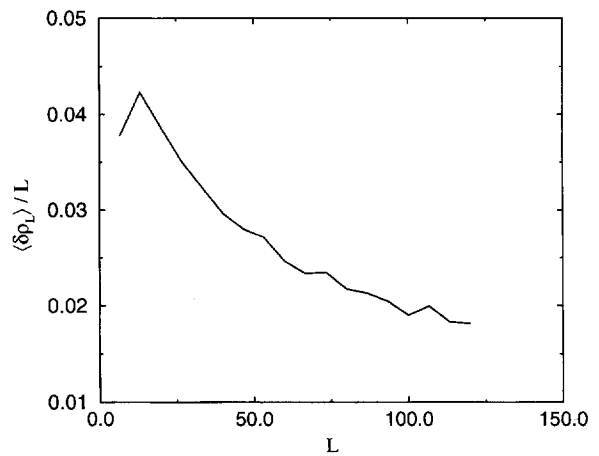

Fig. 3. $\langle \delta\rho_L \rangle / L$ versus L. This was obtained by measuring the excess topological charge (as in Eq. (8)) for 138 different 240 × 240 systems. Each picture was divided into $L \times L$ regions in which $\delta\rho_L$ was calculated. $\langle \delta\rho_L \rangle$ was then obtained by averaging over these regions and over the different pictures. The parameters are $b_x = -0.75$, $b_y = -3.0$, and $c = 1.5$.

from local fluctuations at the perimeter of the box. In order to see this, consider joining each defect to its closest neighbor of opposite sign. Pairs entirely inside the perimeter do not contribute to the excess topological charge, but pairs split by the perimeter can contribute. Now divide the perimeter into sections of fixed length. In each section, the defects in the split pairs remaining inside the box contribute an excess equal to their net topological charge. Note that this number can be either positive or negative. The overall excess $\delta\rho_L$ is the sum of these excesses over all the sections of the perimeter, i.e. it is a sum over random variables with different signs. But this process is just a random walk, and such a process yields a sum that scales as the square root of the number of steps. The number of steps (sections of perimeter) is proportional to the perimeter, so we expect $\langle \delta\rho_L \rangle \sim L^{1/2}$, which is what we found.

In Fig. 4 we present the results for $G_\rho(\boldsymbol{r})$ for $\boldsymbol{r}$ in the $\hat{x}$ and $\hat{y}$ directions. For both directions the typical nearest neighbor is of the opposite sign: the topological charges are screened. Similar behavior for vortices in random wave

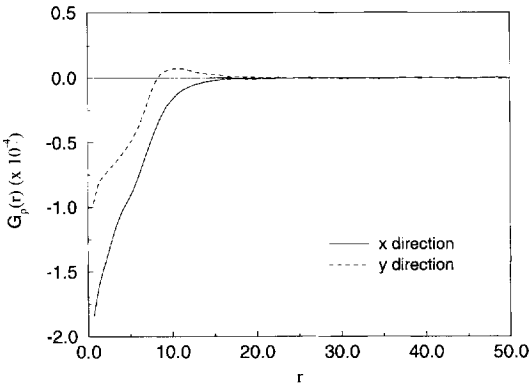

Fig. 4. $G_\rho(\boldsymbol{r})$ versus r. The solid line is for the $\hat{x}$ direction, while the dashed line is for the $\hat{y}$ direction. Also shown is a line for $G = 0$. Note that G attains its asymptotic limit of 0 from different sides of this line for the different directions of $\boldsymbol{r}$. The parameters are $b_x = -0.75$, $b_y = -3.0$, and $c = 1.5$.

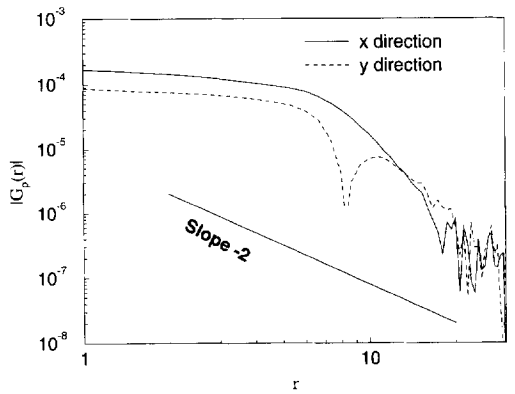

Fig. 5. Log–log plot of $|G_\rho(\boldsymbol{r})|$ versus r. The solid line corresponds to the $\hat{x}$ direction and the dashed line to the $\hat{y}$ direction. Also shown is a line with slope that would correspond to $|G_\rho(r)| \sim 1/r^2$. The parameters are $b_x = -0.75$, $b_y = -3.0$, and $c = 1.5$.

fields has been observed [71]. In Fig. 5 we show log–log plots of $|G_\rho(r)|$. Also shown are lines that represent the slope $|G_\rho(r)|$ would have if it decayed as $1/r^2$. At the right edge of the figure, we have reached the point where our data are dominated by statistical noise. Neither direction strongly shows $1/r^2$ decay, although due to statistical noise the numerical results do not completely rule out such a decay. (We will discuss the issue of statistics which impact our results below.) This lack of strong evidence for $1/r^2$ decay is at variance with the predictions of generic scale invariance, under the assumption that the chaotic fluctuations resemble white noise [6–12]. This numerical result was suggested by the results on topological constraints given in Section 3.

The suggestion has been made [72] that in order to see the $1/r^2$ decay the system needs to break $x \to -x$ symmetry. We tested this idea by adding another term to the original equation (38). This added term, $\mathrm{d}\partial_x(|A|^2 A)$, where d is real, breaks the $x \to -x$ symmetry and *is* also expected to show a $1/r^2$ decay, according to the predictions of generic scale invariance. The numerical results for $G_\rho(r)$ are shown in Fig. 6 for the particular case $d = 1$. Other values of d give similar results. We see from these results that this correlation function also does not suggest $1/r^2$ decay. This result was again suggested by our results from Section 3, which should apply to any two-dimensional topological defect in a complex field.

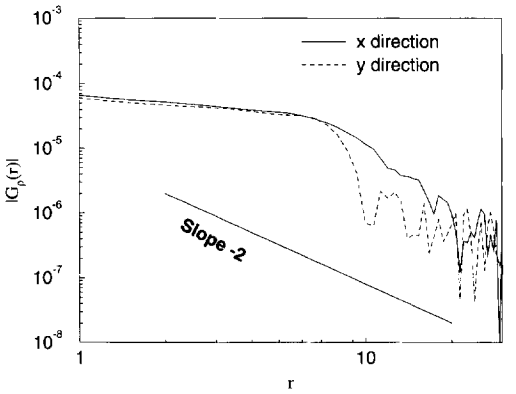

Fig. 6. Log–log plot of $|G_\rho(r)|$ versus r for the case where we have added a term $d\partial_x|A(x,t)|^2A(x,t)$ to the complex Ginzburg–Landau equation. Here we have $d = 1.0$. The solid line corresponds to the $\hat{x}$ direction and the dashed line to the $\hat{y}$ direction. Also shown is a line with slope that would correspond to $|G_\rho(r)| \sim 1/r^2$. The parameters are $b_x = -0.75$, $b_y = -3.0$, and $c = 1.5$.

In addition, as a further test we have added an explicit nonconserving stochastic white noise to the complex Ginzburg–Landau equation. This noise should act like a conserving noise for the topological defects. The results for $|G_\rho(r)|$ in this case were similar to the previous results. We have also experimented with adding various other terms to the original equation. None of these added terms significantly changed the results for the topological defect correlation functions.

The results we have presented for the correlation function are for a microscopic topological order parameter ρ. We can consider what happens when we construct a coarse-grained order parameter field by defining

$$\rho_{cg}(\boldsymbol{r}) \equiv \int \mathrm{d}\boldsymbol{s}\, h(\boldsymbol{s})\rho(\boldsymbol{r}-\boldsymbol{s}) \tag{39}$$

where $h(\boldsymbol{s})$ is a coarse-graining weight function with $\int \mathrm{d}\boldsymbol{s}\, h(\boldsymbol{s}) = 1$. An example of such a function is the Gaussian $h(\boldsymbol{s}) = (1/2\pi\sigma^2)\mathrm{e}^{-s^2/2\sigma^2}$. With this we can also calculate $G_{\rho_{\mathrm{cg}}}(r)$ and examine its behavior at large r. The coarse-grained correlation function is given by

$$G_{\rho_{\mathrm{cg}}}(\boldsymbol{r}) = \langle\rho_{\mathrm{cg}}(\boldsymbol{r})\rho_{\mathrm{cg}}(\boldsymbol{0})\rangle = \int\int \mathrm{d}\boldsymbol{s}\,\mathrm{d}\boldsymbol{s}' h(\boldsymbol{s})h(\boldsymbol{s}')\langle\rho(\boldsymbol{r}-\boldsymbol{s})\rho(-\boldsymbol{s}')\rangle. \tag{40}$$

This can be rewritten as

$$G_{\rho_{\mathrm{cg}}}(\boldsymbol{r}) = \int\int \mathrm{d}\boldsymbol{s}\,\mathrm{d}\boldsymbol{s}' h(\boldsymbol{s})h(\boldsymbol{s}')G_\rho(\boldsymbol{r}-(\boldsymbol{s}-\boldsymbol{s}')). \tag{41}$$

We can expand the microscopic correlation function

$$G_\rho(\boldsymbol{r}-\Delta\boldsymbol{s}) = G_\rho(\boldsymbol{r}) - \frac{\partial G_\rho(\boldsymbol{r})}{\partial r_i}\Delta s_i + \Delta s_i\frac{\partial^2 G_\rho(\boldsymbol{r})}{\partial r_i\partial r_j}\Delta s_j + O((\Delta\boldsymbol{s})^3), \tag{42}$$

where $\Delta\boldsymbol{s} = \boldsymbol{s} - \boldsymbol{s}'$ and i and j run from 1 to 2. Inserting this result into Eq. (41) yields (noting that the linear term in $\Delta\boldsymbol{s}$ is zero due to symmetry) to lowest order

$$G_{\rho_{\mathrm{cg}}}(\boldsymbol{r}) = G_\rho(\boldsymbol{r}) + \frac{\partial^2 G_\rho(\boldsymbol{r})}{\partial r_i\partial r_j}\int\int \mathrm{d}\boldsymbol{s}\,\mathrm{d}\boldsymbol{s}' h(\boldsymbol{s})h(\boldsymbol{s}')\Delta s_i\Delta s_j. \tag{43}$$

If $G_\rho(r)$ decays as $r^{-\alpha}$, then the second term will decay as $r^{-(\alpha+2)}$, so all the higher terms in the expansion will decay faster than the original, microscopic correlation function. This result demonstrates that the coarse-grained

order parameter, which is typically what one is discussing in generic scale invariance, will decay as fast as the microscopic order parameter. If the microscopic order parameter decays faster than $1/r^2$, then the macroscopic one should too.

In order to demonstrate this, we have numerically coarse-grained our system of defects, generating a particular new coarse-grained order parameter ρ_{cg} using a Gaussian $h(s)$. The correlation function for the coarse-grained order parameter always decayed as fast or faster than the correlation function for the underlying order parameter ρ, and was thus also not consistent with the predictions of generic scale invariance.

We noted above that the results do not convincingly rule out $1/r^2$ behavior. However, the proof we have provided in Section 3 shows analytically that the topological nature of the defects precludes $1/r^2$ decay in the correlation function. In addition, another group has reproduced our simulations on a massively parallel supercomputer, obtaining more data. Their results are consistent with ours and also do not strongly suggest $1/r^2$ behavior [73]. In order to conclusively rule out $1/r^2$ behavior, we would need to reduce our statistical noise by a factor of 10 or more. In order to do that, we would need to obtain 100 times as much data as we already have taken. This would require access to very long times on many workstations. For example, to obtain this factor of 100 increase in data would require using 100 typical workstations (e.g. IBM RS/6000 model 550's) for an entire month or more.

As a final comment on the numerical results presented in this section, note that the typical spacing between defects in our parameter regime is fairly large. As a result, we are not able to obtain good statistics for the correlation functions for large r, and we might not have reached the asymptotic regime where generic scale invariance should apply. We could increase the density of defects by changing our parameters, but that would then require more Fourier modes to accurately solve the equation and would increase the necessary CPU time.

6. Conclusions

We have examined the predictions of generic scale invariance [1–3] for topological objects, and shown that, at least in some cases, the predictions of generic scale invariance are not compatible with a topological order parameter.

We have also tested this idea in simulations of the two-dimensional complex Ginzburg–Landau equation, where the results for the order parameter field ρ did not agree with the predictions of generic scale invariance. Our results, while preliminary, do suggest that the the decay of the defect–defect correlation function is not $1/r^2$. This places a limit on the applicability of generic scale invariance. Conversely, the results also place a bound on the types of coarse-grained, statistical theories that can be used to describe spatiotemporally chaotic systems with interacting topological defects.

Acknowledgements

We would like to thank D.A. Egolf, P.C. Hohenberg, J.F. Marko, and M.E.J. Newman for helpful conversations. This work was partly funded by the Hertz Foundation (BWR), the NSF under grant DMR-91-18065 (BWR, JPS), and the Alfred P. Sloan Foundation (EB). We also thank the Cornell Materials Science Center for the use of its computational resources.

References

[1] G. Grinstein, D.-H. Lee and S. Sachdev, Phys. Rev. Lett. 64 (1990) 1927.
[2] G. Grinstein, J. Appl. Phys. 69 (1991) 5441.

[3] G. Grinstein, C. Jayaprakash and J.E.S. Socolar, Phys. Rev. E 48 (1993) 643.
[4] G. Grinstein and D.-H. Lee, Phys. Rev. Lett. 66 (1991) 177.
[5] P.L. Garrido, J.L. Lebowitz, C. Maes and H. Spohn, Phys. Rev. A 42 (1990) 1954.
[6] V. Yakhot, Phys. Rev. A 24 (1981) 642.
[7] S. Zaleski, Physica D 34 (1989) 427.
[8] J. Miller and D.A. Huse, Phys. Rev. E 48 (1993) 2528.
[9] M.S. Bourzutschky and M.C. Cross, Chaos 2 (1992) 173.
[10] R. Bhagavatula, G. Grinstein, Y. He and C. Jayaprakash, Phys. Rev. Lett. 69 (1992) 3483.
[11] H. Chaté, G. Grinstein and L.-H. Tang, Phys. Rev. Lett. 74 (1995) 912.
[12] C. Jayaprakash, F. Hayot and R. Pandit, Phys. Rev. Lett. 71 (1993) 12.
[13] B.M. Law, R.W. Gammon and J.V. Sengers, Phys. Rev. Lett. 60 (1988) 1554.
[14] B.M. Law, P.N. Segrè, R.W. Gammon and J.V. Sengers, Phys. Rev. A 41 (1990) 816.
[15] J.R. Dorfman, T.R. Kirkpatrick and J.V. Sengers, Ann. Rev. Phys. Chem. 45 (1994) 213.
[16] M.C. Cross and P.C. Hohenberg, Science 263 (1994) 1569.
[17] M.C. Cross and P.C. Hohenberg, Rev. Mod. Phys. 65 (1993) 851.
[18] E. Bodenschatz, J. DeBruyn, G. Ahlers and D. Cannell, Phys. Rev. Lett. 67 (1991) 3078.
[19] S.W. Morris, E. Bodenschatz, D.S. Cannell and G. Ahlers, Phys. Rev. Lett. 71 (1993) 2026.
[20] J.R. de Bruyn, E. Bodenschatz, S.W. Morris, S.P. Trainoff, Y. Hu, D.S. Cannell and G. Ahlers, Apparatus for the study of Rayleigh–Bénard convection in gases under pressure, Rev. Sci. Inst. (1996), submitted.
[21] M. Assenheimer and V. Steinberg, Nature 367 (1994) 345.
[22] S. Kai and K. Hirakawa, Suppl. Prog. Theor. Phys. 64 (1978) 212.
[23] I. Rehberg, S. Rasenat and V. Steinberg, Phys. Rev. Lett. 62 (1989) 756.
[24] E. Braun, S. Rasenat and V. Steinberg, Europhysics Lett. 15 (1991) 597.
[25] S. Nasuno and S. Kai, Europhysics Lett. 14 (1991) 779.
[26] S.-I. Sasa, Prog. Theor. Phys. 83 (1990) 824.
[27] N.B. Tufillaro, R. Ramashankar and J.P. Gollub, Phys. Rev. Lett. 62 (1989) 422.
[28] J.M. Davidenko, A.V. Pertsov, R. Salomonsz, W. Baxter and J. Jalife, Nature 355 (1993) 349.
[29] Q. Ouyang and H.L. Swinney, Chaos 1 (1991) 411.
[30] A.C. Newell and J.V. Moloney, Nonlinear Optics (Addison-Wesley, New York, 1992).
[31] J. Lega, J.V. Moloney and A.C. Newell, Phys. Rev. Lett. 73 (1994) 2978 and references therein.
[32] S. Ciliberto and M. Caponeri, Phys. Rev. Lett. 64 (1990) 2775.
[33] P.C. Hohenberg and B.I. Shraiman, Physica D 37 (1989) 109.
[34] C.C. Chow and T. Hwa, Physica D 84 (1995) 494.
[35] M.C. Cross and Y. Tu, Phys. Rev. Lett. 75 (1995) 834.
[36] P. Coullet, L. Gil and J. Lega, Phys. Rev. Lett. 62 (1989) 1619.
[37] P. Coullet, L. Gil and J. Lega, Physica D 37 (1989) 91.
[38] L. Gil, J. Lega and J.L. Meunier, Phys. Rev. A 41 (1990) 1138.
[39] J. Lega, Comput. Methods Appl. Mech. Eng. 89 (1991) 419.
[40] I. Aranson, L. Kramer and A. Weber, Phys. Rev. Lett. 72 (1994) 2316.
[41] A.C. Newell, in: Nonlinear Wave Motion, ed. A.C. Newell (American Mathematical Society, Providence, RI, 1974).
[42] T.B. Benjamin and J.E. Feir, J. Fluid Mech. 27 (1967) 417.
[43] J.T. Stuart and R.C. DiPrima, Proc. Roy. Soc. London Ser. A 362 (1978) 27.
[44] R. Brown, A.L. Fabrikant and M.I. Rabinovich, Phys. Rev. E 47 (1993) 4141.
[45] D. Hansel and H. Sompolinsky, Phys. Rev. Lett. 71 (1993) 2710.
[46] M. Eisele, Physica D 48 (1991) 295.
[47] V. L'vov and I. Procaccia, Phys. Rev. Lett. 72 (1993) 307.
[48] C. Jayaprakash, F. Hayot and R. Pandit, Phys. Rev. Lett. 72 (1993) 308.
[49] P. Minnhagen, Rev. Mod. Phys. 59 (1987) 1001.
[50] E. Butkov, Mathematical Physics (Addison-Wesley, Reading, MA, 1968), Section 6.2, p.223.
[51] Z. Cheng, P.L. Garrido, J.L. Lebowitz and J.L. Vallés, Europhysics Lett. 14 (1991) 507.
[52] M.Q. Zhang, J.-S. Wang, J.L. Lebowitz and J.L. Vallés, J. Stat. Phys. 52 (1988) 1461.
[53] A.P. Prudnikov, Yu. A. Brychkov and O.I. Marichev, Integrals and Series (Gordon and Breach, New York, NY, 1986), Vol. 2, p.232. Note that there is a mistake in the formula given. $(1/\pi)\cos^{-1}(\ ) - c\surd$ should be $(1/\pi)\left(\cos^{-1}(\ ) - c\surd\right)$.
[54] L. Kramer, F. Hynne, P. Graae Sørenson and D. Walgraef, Chaos 4 (1994) 443.
[55] Y. Kuramoto, Chemical Oscillations, Waves and Turbulence (Springer, New York, 1984).
[56] P.S. Hagan, SIAM J. Appl. Math. 42 (1982) 762.
[57] E. Bodenschatz, A. Weber and L. Kramer, in: Nonlinear Wave Processes in Excitable Media, eds. A. Holden, M. Markus and H. Othmer (Plenum Press, New York, 1991).

[58] G. Huber, P. Alstrøm and T. Bohr, Phys. Rev. Lett. 69 (1992) 2380.
[59] H. Sakaguchi, Prog. Theor. Phys. 82 (1989) 7.
[60] S.C. Müller, T. Plesser and B. Hess, Physica D 24 (1987) 71; Physica D 24 (1987) 87.
[61] M.C. Cross and A.C. Newell, Physica D 10 (1984) 299.
[62] A.C. Newell, T. Passot and M. Souli, Phys. Rev. Lett. 64 (1990) 2378; J. Fluid Mech. 220 (1990) 187.
[63] I.S. Aranson, L. Kramer and A. Weber, Phys. Rev. E 47 (1993) 3231.
[64] I.S. Aranson, L. Kramer and A. Weber, Physica D 53 (1991) 376.
[65] C. Canuto, M.Y. Hussaini, A. Quarteroni and T. A. Zang, Spectral Methods in Fluid Dynamics (Springer, New York, 1988).
[66] D. Gottleib and S.A. Orszag, Numerical Analysis of Spectral Methods: Theory and Applications (SIAM, Philadelphia, PA, 1977).
[67] P. Coullet, C. Elphick, L. Gil and J. Lega, Phys. Rev. Lett. 59 (1987) 884.
[68] B.I. Halperin, in: Physics of Defects, eds. R. Balian et al. (North-Holland, New York, 1981).
[69] F. Liu and G.F. Mazenko, Phys. Rev. B 46 (1992) 5963.
[70] M. Mondello and N. Goldenfeld, Phys. Rev. A 42 (1990) 5865.
[71] N. Shvartsman and I. Freund, Phys. Rev. Lett. 72 (1994) 1008; Phys. Rev. Lett. 72 (1994) 4156 (E).
[72] G. Grinstein, private communication.
[73] D.A. Egolf and H.S. Greenside, private communication.